Remote Sensing

Supporting Information for

Accounting for 10 m Resolution Mapping for Above-Ground Biomass of Urban Trees in C40 Cities Across Eurasia Continent

Ge Yan [1,2,3], Zhifang Shi [1,2,3], Gaomin Lian [1,2,3], Kailong Cui [1,2,3,4], Nan Li [5], Ying Luo [6], Shuyuan Zhou [7], Mengmeng Cao [1,2,3,*] and Yaoping Cui [1,2,3]

[1] State Key Laboratory of Spatial Datum, Henan University, Zhengzhou 450046, China; yangeer@henu.edu.cn (G.Y.); shizhifang@henu.edu.cn (Z.S.); gaomin@henu.edu.cn (G.L.); cui@henu.edu.cn (K.C.); cuiyp@lreis.ac.cn (Y.C.)
[2] Faculty of Geographical Science and Engineering, College of Geographical Sciences, Henan University, Zhengzhou 450046, China
[3] Key Laboratory of Geospatial Technology for the Middle and Lower Yellow River Regions, Ministry of Education, Henan University, Kaifeng 475004, China
[4] The State Key Laboratory of Information Engineering in Surveying Mapping and Remote Sensing, Wuhan University, Wuhan 430079, China
[5] School of Geography and Tourism, Zhengzhou Normal University, Zhengzhou 450004, China; linan0716@henu.edu.cn
[6] School of Tourism and Exhibition, Henan University of Economics and Law, Zhengzhou 450004, China; ly_075@163.com
[7] Xun County Bureau of Natural Resources, Hebi 458000, China; 13783000572@163.com
* Correspondence: mmengcao@henu.edu.cn

Contents of this file

Table S1 to S6

Method S1 to S2

Figure S1

Reference

Table S1. Major Köppen-Geiger climatic types with representative C40 Cities.

Climate types	Representative cities	Typical characteristics
Tropical rainforest climate	Singapore, Jakarta, Rio de Janeiro	High temperature and abundant rainfall prevail throughout the year, with a mean annual temperature above 18 ° C and annual precipitation exceeding 2000 mm; the vegetation is mainly evergreen broad-leaved forest.
Tropical savanna climate	Brasília, Mexico, Johannesburg	Distinct wet and dry seasons, with annual precipitation of 800-1500 mm; the vegetation is mainly savanna.
Tropical desert climate	Lima, Dubai	Extremely arid, with annual precipitation below 250 mm; vegetation is sparse and relies on artificial oases.
Mediterranean climate	Rome, Cape Town, Los Angeles	Hot and dry summers, warm and wet winters, with annual precipitation of 300-1000 mm; vegetation is chlorophyll forest or shrub.
Subtropical monsoon climate	Shanghai, Tokyo, Hong Kong	Hot and humid summers, mild and dry winters, with annual precipitation of 1000-2000 mm; vegetation is mainly evergreen broad-leaved forest.
Temperate oceanic climate	London, Paris, Vancouver	Mild and rainy throughout the year, with a small annual temperature range and evenly distributed precipitation; vegetation is mainly deciduous forest.
Temperate monsoon climate	Beijing, Seoul	Hot and humid summers, cold and dry winters, with annual precipitation of 500-1000 mm; vegetation consists of deciduous or mixed coniferous-broad leaf forests.
Temperate continental climate	Chicago, Moscow, Tehran	Large annual temperature range, precipitation concentrated in summer; vegetation is mainly grassland or coniferous forest.
Alpine plateau climate	Quito, Bogotá	Pronounced vertical climate differentiation, mean annual temperature below 10 ° C; vegetation varies with altitude.

Table S2. Sentinel-2 raw image data used for each city.

Continent	City name	Sentinel-2 raw images			
		Year	Cloud cover (%)	Number	Data size (G)
Asia	Ahmadabad	2020	5	35	132.02
	Amman	2020	5	34	135.67
	Bangalore	2020	5	35	132.46
	Bangkok	2020	5	103	389.19
	Beijing	2018-2024	5	16	60.63
	Chengdu	2020	5	61	231.44
	Chennai	2020	5	98	375.39
	Dalian	2020	5	79	301.04
	Delhi	2020	5	18	68.29
	Dhaka	2020	5	220	846.79
	Dubai	2020	5	72	280.55
	Fuzhou	2020	5	57	218.14
	Guangzhou	2020	5	34	121.77
	Hangzhou	2020	5	70	271.84
	Hanoi	2020	5	35	133.64
	Ho Chi Minh	2020	10	85	330.46
	Hongkong	2020	5	37	141.68
	Jakarta	2020	5	53	216.02
	Karachi	2020	5	211	790.78
	Kolkata	2020	5	27	103.58
	Kuala Lumpur	2019	5	54	212.09
	Mumbai	2020	5	39	148.53
	Nanjing	2020	5	70	264.96
	Qingdao	2020	5	17	63.88
	Quezon	2020	5	99	372.55
	Seoul	2020	5	136	517.26

Table S2. continued.

Continent	City name	Sentinel-2 raw images			
		Year	Cloud cover (%)	Number	Data size (G)
Asia	Shanghai	2020	5	37	140.25
	Shenzhen	2020	5	52	182.21
	Singapore	2023	10	101	377.81
	Tel Aviv Yafo	2020	5	52	205.52
	Tokyo	2020	5	34	128.49
	Wuhan	2020	5	103	388.02
	Yokohama	2020	5	55	208.19
	Zhenjiang	2020	5	36	137.06
Europe	Amsterdam	2020	5	140	526.17
	Athens	2020	5	231	867.98
	Barcelona	2020	5	214	803.57
	Berlin	2020	5	204	770.76
	Copenhagen	2020	5	158	578.82
	Heidelberg	2020	5	103	389.32
	Istanbul	2020	5	90	351.86
	Lisboa	2020	5	175	656.9
	London	2020	5	194	751.85
	Madrid	2020	5	192	723.21
	Milano	2020	5	160	608.49
	Oslo	2020	5	190	704.9
	Paris	2020	5	107	404.12
	Roma	2020	5	243	912.02
	Rotterdam	2020	5	158	594.74
	Stockholm	2020	5	186	622.47
	Warsaw	2020	5	141	531.32

Table S3. Configuration of random forest model hyperparameters.

Hyperparameter	Parameter Search Range	Optimal Hyperparameter
min_samples_leaf	[5, 10,15, 30, 60]	15
min_samples_split	[5, 10,15, 30, 60]	10
max_depth	[2, 4, 6, 8, 10]	6
n_estimators	[50, 200, 600, 800, 1000]	800

Table S4. Vegetation indices and calculation formulas used in this study.

ID	Name	Formula	Ref
1	Normalized Difference Vegetation Index (NDVI)	NDVI = (NIR - Red) / (NIR + Red)	[1]
2	Green Normalized Difference Vegetation Index (GNDVI)	GNDVI = (NIR - Green) / (NIR + Green)	[2]
3	Renormalized Difference Vegetation Index (RDVI)	RDVI = (NIR - Red) / sqrt(NIR + Red)	[2]
4	Enhanced Vegetation Index (EVI)	EVI = 2.5 × ((NIR - Red) / (NIR + 6 × Red - 7.5 × Blue + 1))	[3]
5	Enhanced Vegetation Index 2 (EVI2)	EVI2 = 2.5 × ((NIR - Red) / (NIR + 2.4 × Red + 1))	[1]
6	Enhanced Vegetation Index for Red Edge 1 (EVI_RE1)	EVI_RE1 = 2.5 × ((NIR - RE1) / (NIR + 6 × RE1 - 7.5 × Blue + 1))	[4,5]
7	Enhanced Vegetation Index for Red Edge 2 (EVI_RE2)	EVI_RE2 = 2.5 × ((NIR - RE2) / (NIR + 6 × RE2 - 7.5 × Blue + 1))	[4,5]
8	Enhanced Vegetation Index for NIR 1 (EVI_NIRn1)	EVI_NIRn1 = 2.5 × ((NIR1 - Red) / (NIR1 + 6 × Red - 7.5 × Blue + 1))	[4,5]

9	Enhanced Vegetation Index for NIR 2 (EVI_NIRn2)	EVI_NIRn2 = 2.5 × ((NIR2 - Red) / (NIR2 + 6 × Red - 7.5 × Blue + 1))	[4,5]
10	Green Chlorophyll Index (GCI)	GCI = (NIR - Green) / (NIR + Green)	[6]
11	Atmospherically Resistant Vegetation Index (ARVI)	ARVI = (NIR - (Red + Blue)) / (NIR + (Red + Blue))	[7]
12	Visible Atmospherically Resistant Index (VARI)	VARI = (Green - Red) / (Green + Red - Blue)	[8]
13	Soil Adjusted Vegetation Index (SAVI)	SAVI = (NIR - Red) / (NIR + Red + L) × (1 + L)	[1]

Table S4. continued.

ID	Name	Formula	Ref
14	Optimized Soil-Adjusted Vegetation Index (OSAVI)	OSAVI = (NIR - Red) / (NIR + Red + 0.16) × (1 + 0.16)	[9]
15	Modified Soil-Adjusted Vegetation Index (MSAVI)	MSAVI = (2 × NIR + 1 - sqrt((2 × NIR + 1)2 - 8 × (NIR - Red))) / 2	[9]
16	Normalized Difference Infrared Index (NDII)	NDII = (NIR - SWIR) / (NIR + SWIR)	[10,11]
17	Normalized Difference Infrared Index 2 (NDII2)	NDII2 = (NIR - SWIR2) / (NIR + SWIR2)	[10,11]
18	Difference Vegetation Index (DVI)	DVI = NIR - Red	[2]
19	Normalized Green-Red Difference Index (NGRDI)	NGRDI = (Green - Red) / (Green + Red)	[1]
20	Atmospheric Vegetation Index (AVI)	AVI = (NIR - Red) / (NIR + Red)	[12]
21	Normalized Difference Vegetation Index for Red Edge	NDVIre = (NIR - RE) / (NIR + RE)	[13,14]

	(NDVIre)		
22	Modified Normalized Difference Vegetation Index (MNDVI)	MNDVI = (NIR - Red) / (NIR + Red)	[2]
23	Red-Edge Vegetation Index (RTVI)	RTVI = (NIR - RE) / (NIR + RE)	[15]
24	Simple Ratio Red-Edge (SRre)	SRre = NIR / RE	[16]
25	Red Edge Chlorophyll Index (RECI)	RECI = (NIR - RE) / (NIR + RE)	[6]

Table S4. continued.

ID	Name	Formula	Ref
26	Green Atmospherically Resistant Index (GARI)	GARI = (Green - Red) / (Green + Red)	[17]
27	Green Difference Vegetation Index (GDVI)	GDVI = Green - Red	[18]
28	Infrared Red Edge Chlorophyll Index (IRECI)	IRECI = (NIR - RE) / (NIR + RE)	[19,20]
29	Modified Chlorophyll Absorption Ratio Index (MCARI)	MCARI = (NIR - RE) / (NIR + RE)	[21]
30	Moisture Stress Index (MSI)	MSI = SWIR / NIR	[22]
31	Modified Simple Ratio (MSR)	MSR = (NIR - Red) / (NIR + Red)	[22]
32	Modified Simple Ratio Red Edge 1 (MSR_RE1)	MSR_RE1 = (NIR - RE1) / (NIR + RE1)	[23,24]

33	Modified Simple Ratio Red Edge 2 (MSR_RE2)	MSR_RE2 = (NIR - RE2) / (NIR + RE2)	[23,24]
34	Modified Simple Ratio NIR 1 (MSR_NIR1)	MSR_NIR1 = (NIR1 - Red) / (NIR1 + Red)	[25]
35	Modified Simple Ratio NIR 2 (MSR_NIR2)	MSR_NIR2 = (NIR2 - Red) / (NIR2 + Red)	[25]
36	Normalized Difference Water Index (NDWI)	NDWI = (Green - NIR) / (Green + NIR)	[1]
37	Normalized Green (NG)	NG = Green / (Green + Red + NIR)	[26]
38	Non-Linear Index (NLI)	NLI = (NIR - Red) / (NIR + Red)	[27]

Table S4. continued.

ID	Name	Formula	Ref
39	Normalized Near-Infrared Index (NNIR)	NNIR = NIR / (Red + Green + Blue)	[26]
40	Normalized Red (NR)	NR = Red / (Red + Green + Blue)	[26]
41	Plant Senescence Reflectance Index (PSRI)	PSRI = (Red - Green) / (Red + Green)	[28]
42	NIR Plant Senescence Reflectance Index (NIRPSRI)	NIRPSRI = (NIR - Red) / (NIR + Red)	[28]
43	Pigment Specific Simple Ratio (PSSR)	PSSR = (NIR - Red) / (NIR + Red)	[19]
44	Transformed Soil-Adjusted Vegetation Index (TSAVI)	TSAVI = (NIR – a) × (Red - b) / (NIR + a) × (Red + b)	[29]
45	Wide Dynamic Range Vegetation Index (WDRVI)	WDRVI = (NIR - Red) / (NIR + Red)	[30]

46	Wide Dynamic Range Vegetation Index (KNDVI)	KNDVI = (NIR - Red) / (NIR + Red)	[31]

Table S5. Texture features and their calculation formulas used in this study.

Name	Formula	Description
Angular Second Moment (ASM)	$\mathrm{ASM} = \sum_{i=0}^{N-1}\sum_{j=0}^{N-1} P(i,j)^2$	This index quantifies the uniformity of gray-level distribution in an image, with higher values indicating greater spatial consistency of pixel values.
Variance (VAR)	$\mathrm{VAR} = \sum_{i=0}^{N-1}\sum_{j=0}^{N-1} (i-\mu)^2 \cdot P(i,j)$	This index quantifies surface structural heterogeneity, with high variance indicating canopy gaps or areas near non-vegetated regions.
Inverse Difference Moment (IDM)	$\mathrm{IDM} = \sum_{i=0}^{N-1}\sum_{j=0}^{N-1} \frac{P(i,j)}{1+(i-j)^2}$	This index increases with decreasing pixel-to-pixel differences and is particularly sensitive to distinguishing natural vegetation from artificial impervious surfaces.
Contrast (CON)	$\mathrm{CON} = \sum_{i=0}^{N-1}\sum_{j=0}^{N-1} (i-j)^2 \cdot P(i,j)$	This index quantifies the intensity of gray-level differences between adjacent pixels. High-contrast areas typically correspond to object boundaries or abrupt reflectance changes.
Dissimilarity (DISS)	$\mathrm{DISS} = \sum_{i=0}^{N-1}\sum_{j=0}^{N-1} \lvert i-j\rvert \cdot P(i,j)$	Similar to contrast, this index is more sensitive to moderate gray-level variations, aiding the identification of micro-structures in fragmented green spaces or small forest patches.
Entropy (ENT)	$\mathrm{ENT} = -\sum_{i=0}^{N-1}\sum_{j=0}^{N-1} P(i,j) \cdot \log P(i,j)$	This index characterizes the spatial heterogeneity of forest canopy structure, with high-entropy areas generally indicating greater potential

		for biomass accumulation.
Sum Average (SAVG)	$\mathrm{ASAVG} = \sum_{k=2}^{2N} k \cdot P_{x+y}(k)$	This index assigns higher values to high-reflectance surfaces and lower values to vegetated areas, and can compensate for classification errors in spectral indices due to radiometric distortions.
Correlation (CORR)	$\mathrm{CORR} = \sum_{i=0}^{N-1} \sum_{j=0}^{N-1} \frac{(i-\mu_i)(j-\mu_j)P(i,j)}{\sigma_i \sigma_j}$	This index represents the linear dependency between pixels, with high values typically indicating regularly patterned textures.

Variable types	Variable Components	Number
Vegetation Indices	NDVI, GNDVI, RDVI, EVI, EVI2, EVI_RE1, EVI_RE2, EVI_NIRn1, EVI_NIRn2, GCI, ARVI, VARI, SAVI, etc.	46
Sentinel-2 raw bands	B1, B2, B3, B4, B5, B6, B7, B8, B8A, B9, B10, B11, B12	13
Texture features	ASM, VAR, IDM, CON, DISS, ENT, SAVG, CORR, derived from 10 spectral bands and1 fused grayscale band of Sentinel-2, respectively.	88
Other	Sentinel-2 fused grayscale band	1
	Tree canopy height fusion data with 10 m resolution	1
	Total	149

Method S1. Urban Trees Outside Forests (TOF) data extraction.

The urban Trees Outside Forests (TOF) were classified and extracted according to the biophysical thresholds defined by the Global Forest Resources Assessments of the United Nations Food and Agricultural Organization. The specific classification rules were as follows: Within urban areas, patches with canopy height (CH) > 5 m, fractional vegetation cover (FVC) ≥ 20%, and area (A) ≥ 0.5 ha were classified as urban forest; CH > 5 m, FVC ≤ 20%, and A < 0.5 ha were classified as urban tree; and 1 m ≤ CH < 5 m were classified as urban shrub. Within cropland areas, 2 m ≤ CH < 5 m patches were classified as cropland shrub.

Method S2. 10 m Canopy Height Data Construction.

The 10 m canopy height (CH-10m) vegetation data from the ETH Global Sentinel-2 dataset published by Eidgenössische Technische Hochschule Zürich (ETH Zürich) (https://nlang.users.earthengine.app/view/global-canopy-height-2020), and the global 1 m canopy height (CH-1m) data released by Meta and the World Resources Institute (WRI) (https://registry.opendata.aws/dataforgood-fb-forests/) were used to construct a new dataset of canopy height at 10 m resolution.

CH-10m provides extensive spatial coverage but cannot clearly capture fine-scale local variations, especially in low-canopy or densely vegetated areas. In contrast, CH-1m offers higher spatial resolution but may contain data gaps or missing values in some regions, leading to incomplete canopy height information at certain locations. To overcome the limitations of these two datasets, we fused them into a new canopy height product (CH-new). First, the CH-1m data were resampled to 10 m resolution to ensure consistency with the ETH CH-10m dataset. Next, overlapping regions within C40 urban areas were identified through spatial overlay analysis. Finally, a maximum value fusion method was applied, allowing CH-new to retain the fine-grained details of CH-1m while maintaining the broad coverage of CH-10m.

The precision of CH-new was validated through visual and qualitative comparisons (Figure S1). Across various urban landscapes and at different resolutions, CH-new consistently outperforms both CH-1m and CH-10m. In key regions (marked by red boxes), CH-new maximizes the accuracy of fine-scale details while preserving

macro-scale spatial information, effectively balancing data completeness and reliability. The dataset is scheduled for public release soon.

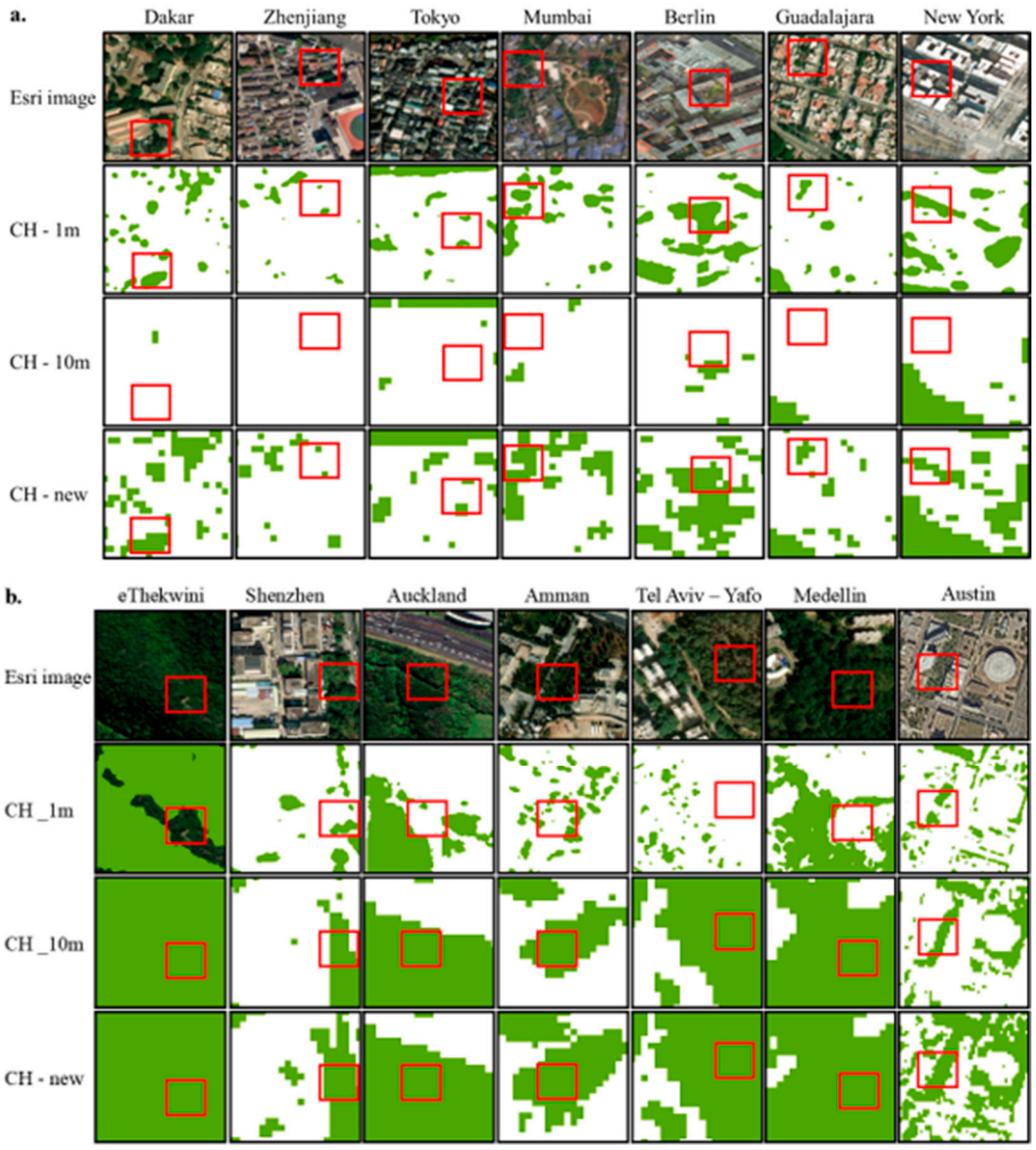


Figure S1. Differences in the representation of urban TOF features by canopy height data at different resolutions; (a) low resolution; (b) high resolution.

Reference

1. Xue, J.; Su, B. Significant remote sensing vegetation indices: A review of developments and applications. *Journal of sensors* **2017**, *2017*, 1353691.
2. Dong, T.; Meng, J.; Shang, J.; Liu, J.; Wu, B.; Huffman, T. Modified vegetation indices for estimating crop fraction of absorbed photosynthetically active radiation. *International Journal of Remote Sensing* **2015**, *36*, 3097-3113.
3. Matsushita, B.; Yang, W.; Chen, J.; Onda, Y.; Qiu, G. Sensitivity of the enhanced vegetation index (EVI) and normalized difference vegetation index (NDVI) to topographic effects: a case study in high-density cypress forest. *Sensors* **2007**, *7*, 2636-2651.
4. Nandy, S.; Srinet, R.; Padalia, H. Mapping forest height and aboveground biomass by integrating ICESat-2, Sentinel-1 and Sentinel-2 data using Random Forest algorithm in northwest Himalayan foothills of India. *Geophysical Research Letters* **2021**, *48*, e2021GL093799.
5. Huete, A.; Didan, K.; Miura, T.; Rodriguez, E.P.; Gao, X.; Ferreira, L.G. Overview of the radiometric and biophysical performance of the MODIS vegetation indices. *Remote sensing of environment* **2002**, *83*, 195-213.
6. Nadjla, B.; Assia, S.; Ahmed, Z. Contribution of spectral indices of chlorophyll (RECl and GCI) in the analysis of multi-temporal mutations of cultivated land in the Mostaganem plateau. In Proceedings of the 2022 7th international conference on image and signal processing and their applications (ISPA), 2022; pp. 1-6.
7. Lemenkova, P.; Debeir, O. Computing vegetation indices from the satellite images using GRASS GIS scripts for monitoring mangrove forests in the coastal landscapes of Niger Delta, Nigeria. *Journal of Marine Science and Engineering* **2023**, *11*, 871.
8. Stow, D.; Niphadkar, M.; Kaiser, J. MODIS-derived visible atmospherically resistant index for monitoring chaparral moisture content. *International journal of remote sensing* **2005**, *26*, 3867-3873.
9. Kimura, R.; Okada, S.; Miura, H.; Kamichika, M. Relationships among the leaf area index, moisture availability, and spectral reflectance in an upland rice field. *Agricultural Water Management* **2004**, *69*, 83-100.
10. Wilson, N.R.; Norman, L.M. Analysis of vegetation recovery surrounding a restored wetland using the normalized difference infrared index (NDII) and normalized difference vegetation index (NDVI). *International Journal of Remote Sensing* **2018**, *39*, 3243-3274.
11. Yue, J.; Yao, Y.; Shen, J.; Li, T.; Xu, N.; Feng, H.; Wei, Y.; Xu, X.; Lin, Y.; Guo, W. Winter wheat harvest detection via Sentinel-2 MSI images. *International Journal of Remote Sensing* **2025**, *46*, 2482-2500.
12. Bannari, A.; Morin, D.; Bonn, F.; Huete, A. A review of vegetation indices. *Remote sensing reviews* **1995**, *13*, 95-120.
13. Liu, M.; Zhan, Y.; Li, J.; Kang, Y.; Sun, X.; Gu, X.; Wei, X.; Wang, C.; Li, L.; Gao, H. Validation of red-edge vegetation indices in vegetation classification in tropical monsoon region—a case study in Wenchang, Hainan, China. *Remote*

Sensing **2024**, *16*, 1865.
14. Zhang, H.; Li, J.; Liu, Q.; Lin, S.; Huete, A.; Liu, L.; Croft, H.; Clevers, J.G.; Zeng, Y.; Wang, X. A novel red-edge spectral index for retrieving the leaf chlorophyll content. *Methods in Ecology and Evolution* **2022**, *13*, 2771-2787.
15. Magney, T.S.; Eitel, J.U.; Vierling, L.A. Mapping wheat nitrogen uptake from RapidEye vegetation indices. *Precision Agriculture* **2017**, *18*, 429-451.
16. Sharifi, A. Using sentinel-2 data to predict nitrogen uptake in maize crop. *IEEE Journal of Selected Topics in Applied Earth Observations and Remote Sensing* **2020**, *13*, 2656-2662.
17. Gitelson, A.A.; Kaufman, Y.J.; Merzlyak, M.N. Use of a green channel in remote sensing of global vegetation from EOS-MODIS. *Remote sensing of Environment* **1996**, *58*, 289-298.
18. Wu, W. The generalized difference vegetation index (GDVI) for dryland characterization. *Remote Sensing* **2014**, *6*, 1211-1233.
19. Frampton, W.J.; Dash, J.; Watmough, G.; Milton, E.J. Evaluating the capabilities of Sentinel-2 for quantitative estimation of biophysical variables in vegetation. *ISPRS journal of photogrammetry and remote sensing* **2013**, *82*, 83-92.
20. Majasalmi, T.; Rautiainen, M. The potential of Sentinel-2 data for estimating biophysical variables in a boreal forest: A simulation study. *Remote Sensing Letters* **2016**, *7*, 427-436.
21. Dong, T.; Meng, J.; Shang, J.; Liu, J.; Wu, B. Evaluation of chlorophyll-related vegetation indices using simulated Sentinel-2 data for estimation of crop fraction of absorbed photosynthetically active radiation. *IEEE Journal of Selected Topics in Applied Earth Observations and Remote Sensing* **2015**, *8*, 4049-4059.
22. Guan, Q.; Huang, W.; Zhao, J.; Liu, L.; Liang, D.; Huang, L.; Wang, L.; Yang, G. Quantitative identification of yellow rust, powdery mildew and fertilizer-water stress in winter wheat using in-situ hyperspectral data. *Sensor Letters* **2014**, *12*, 876-882.
23. Xu, D.; Zhang, M. Mapping paddy rice using an adaptive stacking algorithm and Sentinel-1/2 images based on Google Earth Engine. *Remote Sensing Letters* **2022**, *13*, 373-382.
24. Xie, Q.; Dash, J.; Huang, W.; Peng, D.; Qin, Q.; Mortimer, H.; Casa, R.; Pignatti, S.; Laneve, G.; Pascucci, S. Vegetation indices combining the red and red-edge spectral information for leaf area index retrieval. *IEEE Journal of selected topics in applied earth observations and remote sensing* **2018**, *11*, 1482-1493.
25. Fernández-Manso, A.; Fernández-Manso, O.; Quintano, C. SENTINEL-2A red-edge spectral indices suitability for discriminating burn severity. *International journal of applied earth observation and geoinformation* **2016**, *50*, 170-175.
26. Radočaj, D.; Šiljeg, A.; Marinović, R.; Jurišić, M. State of major vegetation indices in precision agriculture studies indexed in web of science: A review. *Agriculture* **2023**, *13*, 707.
27. Feng, W.; Wu, Y.; He, L.; Ren, X.; Wang, Y.; Hou, G.; Wang, Y.; Liu, W.; Guo, T. An optimized non-linear vegetation index for estimating leaf area index in winter

wheat. *Precision Agriculture* **2019**, *20*, 1157-1176.
28. Ren, S.; Chen, X.; An, S. Assessing plant senescence reflectance index-retrieved vegetation phenology and its spatiotemporal response to climate change in the Inner Mongolian Grassland. *International journal of biometeorology* **2017**, *61*, 601-612.
29. Rondeaux, G.; Steven, M.; Baret, F. Optimization of soil-adjusted vegetation indices. *Remote sensing of environment* **1996**, *55*, 95-107.
30. Gitelson, A.A. Wide dynamic range vegetation index for remote quantification of biophysical characteristics of vegetation. *Journal of plant physiology* **2004**, *161*, 165-173.
31. Schiefer, F.; Schmidtlein, S.; Frick, A.; Frey, J.; Klinke, R.; Zielewska-Büttner, K.; Junttila, S.; Uhl, A.; Kattenborn, T. UAV-based reference data for the prediction of fractional cover of standing deadwood from Sentinel time series. *ISPRS Open Journal of Photogrammetry and Remote Sensing* **2023**, *8*, 100034.